encit 2020

ABCM Associação Brasileira de Engenharia e Ciências Mecânicas

18th Brazilian Congress of Thermal Sciences and Engineering
November 16–20, 2020 (Online)

ENC-2020-0087
THERMAL ANALYSIS OF HYPERSONIC REACTIVE FLOWS IN THERMODYNAMIC NON-EQUILIBRIUM OVER THE BRAZILIAN REENTRY SATELLITE SARA

Farney Coutinho Moreira, farney.coutinho@gmail.com
William Roberto Wolf, wolf@fem.unicamp.br
University of Campinas - School of Mechanical Engineering

João Luiz F. Azevedo
Institute of Aeronautics and Space - Aerodynamics Division
joaoluiz.azevedo@gmail.com

Abstract. *Numerical simulations of air flows are presented for the Brazilian satellite SARA (Portuguese abbreviation for Satélite de Reentrada Atmosférica) configuration under hypersonic conditions during its reentry. Despite the low density flows, the medium can be modeled as continuum, and the laminar flow approximation is valid. The finite volume method is used to solve the Navier-Stokes equations including Park's two-temperature model for chemical dissociation and ionization. Results are presented in terms of translational-rotational and vibrational-electronic temperature modes and mass fraction distribution along the axisymmetric line of flow stagnation. It is shown that thermodynamic non-equilibrium conditions result from the present high-enthalpy flows.*

Keywords: *Thermodynamic non-equilibrium, heat transfer, hypersonic flow, chemical reactions*

1. INTRODUCTION

Atmospheric reentry has always been a topic of interest in engineering inherent to space exploration. Typically, spacecraft and satellites that perform reentry maneuvers do so at a speed of the order of 10 km/s reaching Mach numbers higher than 20. When initiating the atmospheric reentry procedure at altitudes above 100 km, the spacecraft and crew are not yet subjected to large drag loads since the atmosphere is extremely thin and friction is practically nonexistent. As altitude is reduced in the descent procedure, the atmosphere becomes denser and the flow is hypersonic. In this regime, typically observed for Mach numbers $M_\infty > 5$, high-temperature shock layers are formed close to the vehicle surface leading to vibrational excitation of molecules and chemical reactions. Reentry space vehicles and satellites have a large amount of stored kinetic energy and, in order to be able to land safely on the Earth surface (or even in another planet with a different atmosphere), it is necessary to decelerate the vehicle. This process transforms kinetic and potential energy into thermal energy which is, then, transferred to the vehicle surface as heat.

The effects of chemical reaction models in hypersonic flow simulations have been investigated by several authors. Wang *et al.* (2017) assess the performance of four chemical kinetic models for the computation of heat transfer on hypersonic vehicles of different geometrical complexities. They found that all models studied provide good agreement to experimental data for simpler geometries while discrepancies are observed for more complex configurations, especially in terms of the peak heat flux. The performance of three chemical models is investigated by Niu *et al.* (2018) with a special attention to the non-equilibrium weight factor that ponderates the importance of the translational-rotational and vibrational-electronic temperatures. Recently, Kim *et al.* (2020) proposed a modified non-equilibrium model for oxygen that is important to hypersonic cruise vehicles. Reacting gas-surface interactions were studied in Yang *et al.* (2020) and Bouyahiaoui *et al.* (2020) for flows of carbon dioxide, which provide a good model of Mars' atmosphere. These authors investigated the effects of surface catalicity and showed that near-wall diffusion and chemical reactions play an important role in the flow structure along the boundary layer, modifying the surface heat transfer. Studies of ablative surfaces have also been considered in Yang *et al.* (2020) and Riccio *et al.* (2017).

In the present work, we simulate hypersonic flows over the Brazilian satellite SARA. An overall view of the 3D model is presented in Fig. 1(a) while Fig. 1(b) shows geometrical details of the satellite. Although several studies have been performed of hypersonic flows over complex configurations, the literature is scarce for high-enthalpy conditions over the SARA configuration. Here, we present an assessment of the gas dissociation effects for different flow conditions during the reentry trajectory of the SATA satellite. Moreover, the impact of thermodynamic non-equilibrium conditions will be also discussed.

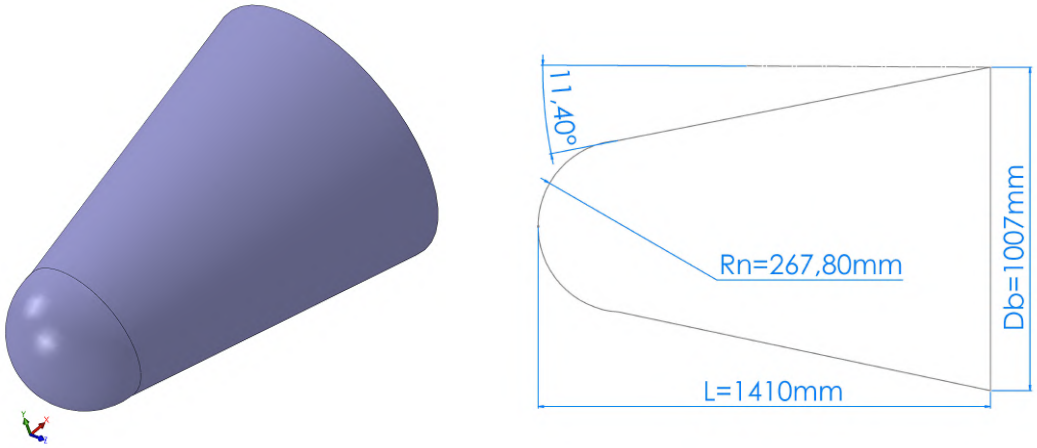

(a) 3D geometry (b) 2D view of geometry with dimensions

Figure 1. Geometry of the Brazilian satellite SARA.

2. THEORETICAL FORMULATION

In the simulations investigated in this work, the flows are modeled as continuum since we expect the maximum Knudsen numbers to be of order 10^{-1}. Hence, the Navier-Stokes equations constitute an accurate model for the present high-enthalpy continuum flows. These equations are solved using Park's two-temperature model to account for thermodynamic non-equilibrium and weak ionization effects (Park, 1988). Hence, it is assumed that the rotational and translational energy modes of all species can be described by a single temperature T_{tr} and that the vibrational energy mode of all species plus the electron energy can also be described by a single temperature T_{ve} (Scalabrin, 2007; Martin *et al.*, 2012).

Through the Boltzmann equation and the Chapman-Enskog theory (Bobylev, 1982), it is possible to obtain the system of conservation equations for transport of mass, momentum and energy, which are herein referred to as Navier-Stokes equations. Here, this system of conservation equations contains a source term that represents chemical reactions including dissociation and ionization under thermodynamic non-equilibrium. A second source term also appears for the present axisymmetric flows. The equations can be written in multi-dimensional form using index notation as follows

$$\frac{\partial Q}{\partial t} + \frac{\partial (F_j - F_{v_j})}{\partial x_j} = S_{cv} + S_{axi}\,, \tag{1}$$

where Q represents the vector of conserved variables, defined as

$$Q = \left\{ \begin{array}{ccccccc} \rho_1 & \ldots & \rho_N & \rho u_i & E & E_{ve} \end{array} \right\}^T. \tag{2}$$

Here, index notation has been used and repeated indices imply summation while a free index represents a vectorial equation. In the vector Q, the terms ρ_1, ..., ρ_N represent the densities of the N chemical species present in the gas mixture. The macroscopic flow velocity components are represented by u_i, the total energy per unit volume is described by E, and the electronic vibrational energy per unit volume of the mixture is represented by E_{ve}.

The components in the j direction of the inviscid F_j and viscous F_{v_j} flux terms are defined as

$$F_j = \left\{ \begin{array}{c} \rho_1 u_j \\ \vdots \\ \rho_N u_j \\ \rho u_i u_j + p\delta_{ij} \\ (E+p)u_j \\ E_{ve} u_j \end{array} \right\} \quad \text{and} \quad F_{v_j} = \left\{ \begin{array}{c} -J_{1,j} \\ \vdots \\ -J_{N,j} \\ \tau_{ij} \\ \tau_{ij} u_i - (q_{tr,j} + q_{ve,j}) - \sum (J_{s,j} h_s) \\ -q_{ve,j} - \sum (J_{s,j} e_{ve,s}) \end{array} \right\}. \tag{3}$$

In the above equations, the variable p represents the mixture pressure and δ_{ij} is the Kronecker delta. According to Fick's Law, the diffusion flux of chemical species s in the j direction is represented by $J_{s,j} = \rho D_s \frac{\partial Y_s}{\partial x_j}$, and the viscous stress tensor components are defined by τ_{ij}. Here, D_s and Y_s represent the diffusion coefficient and molar fraction of species s, respectively. The thermal flux from translational-rotational energy in the j direction is given by $q_{tr,j}$ while $q_{ve,j}$ represents the thermal flux component from electronic-vibrational energy in the j direction, and h_s represents the enthalpy of the chemical species.

The heat fluxes are modeled according to Fourier's law as

$$q_{tr,j} = -k_{tr}\frac{\partial T_{tr}}{\partial x_j} \qquad \text{and} \qquad q_{ve,j} = -k_{ve}\frac{\partial T_{ve}}{\partial x_j} \; . \tag{4}$$

The thermal conductivity of the mixture for each energy mode is calculated using the approach proposed by Eucken (Vincenti and Kruger, 1982). Hence, the conductivity of the translational-rotational and vibrational-electronic modes is computed by

$$k_{tr,s} = \frac{5}{2}\mu_s Cv_{tr,s} + \mu_s Cv_{ve,s} \tag{5}$$

and

$$k_{ve,s} = \mu_s Cv_{ve,s} \; , \tag{6}$$

respectively. Here, $Cv_{tr,s}$ is the constant volume specific heat related to translational-rotational temperature and $Cv_{ve,s}$ is the constant volume specific heat related to vibrational-electronic temperature of chemical species s. The mixture transport properties are modeled using Wilke's semi-empirical mixing rule (Wilke, 1950), as

$$\mu = \sum_s \frac{Y_s \mu_s}{\phi_s} \; , \tag{7}$$

and

$$k = \sum_s \frac{Y_s k_s}{\phi_s} \; . \tag{8}$$

The parameters μ_s and k_s represent the viscosity coefficient and thermal conductivity for an individual species s and the term ϕ_s is calculated using

$$\phi_s = \sum_r Y_r \frac{\left[1 + \sqrt{\frac{\mu_s}{\mu_r}}\left(\frac{M_r}{M_s}\right)^{1/4}\right]^2}{\sqrt{8\left(1 + \frac{M_s}{M_r}\right)}} \; . \tag{9}$$

In the equation above, μ_r and M_r are the viscosity coefficient and molecular weight, respectively, of species r involved in the binary collision with species s. These values can be found in Scalabrin (2007).

In equation 1, the source term S_{cv} represents the rates of mass production of species during chemical reactions. This term is modeled by

$$S_{cv} = \left\{ \; \dot{\omega}_1 \quad \ldots \quad \dot{\omega}_N \quad 0 \quad 0 \quad 0 \quad 0 \quad \dot{\omega}_v \; \right\}^T \; , \tag{10}$$

where $\dot{\omega}_v$ is the vibrational energy source, and $\dot{\omega}_1$, ..., $\dot{\omega}_N$ represent the mass production rates of the N species s due to chemical reactions r.

The chemical reactions of dissociation and ionization can be represented by the following equation

$$\sum \alpha_{rs} \left[S\right] \rightleftharpoons \sum \beta_{rs} \left[S\right] \qquad . \tag{11}$$

Here, $[S]$ represents the chemical species, α_{rs} and β_{rs} are the reagents and products of the stoichiometric coefficients, respectively. The reactions are written such that the right arrow represents an exothermic reaction. The rate of chemical production of species $[S]$ in reaction r is given by

$$\dot{\omega}_s = M_s \sum_{r=1}^{nr} \left(\beta_{rs} - \alpha_{rs}\right) \left[k_{fr} \prod_{s=1}^{N} \left(\frac{\rho_s}{M_s}\right)^{\alpha_{rs}} - k_{br} \prod_{s=1}^{N} \left(\frac{\rho_s}{M_s}\right)^{\beta_{rs}} \right] \qquad , \tag{12}$$

where k_{fr} and k_{br} are the forward and backward reaction rates. The latter depends on the equilibrium constants k_{eq} (Park, 1993) as

$$k_{br} = \frac{k_{fr}\left(T_c\right)}{k_{eq}\left(T_c\right)} \qquad , \tag{13}$$

Table 1. Forward reaction rate coefficients for air flow composed of N_2 and O_2 (cm^3/mole/s) Park (1993).

Reaction	$A(m^3/mole/s)$	η_k	$\theta_r(K)$
Electron Impact Dissociation			
$N_2 + e \rightleftharpoons N + N + e$	$3.0E+24$	-1.60	113200
Dissociation			
$N_2 + M \rightleftharpoons N + N + M(M = N_2, O_2, NO)$	$7.0E+21$	-1.60	113200
$N_2 + M \rightleftharpoons N + N + M(M = N, O)$	$3.0E+22$	-1.60	113200
$N_2 + M \rightleftharpoons N + N + M(M = N_2^+, O_2^+, NO^+)$	$7.0E+21$	-1.60	113200
$N_2 + M \rightleftharpoons N + N + M(M = N^+, O^+)$	$3.0E+22$	-1.60	113200
$O_2 + M \rightleftharpoons O + O + M(M = N_2, O_2, NO)$	$2.0E+21$	-1.50	59500
$O_2 + M \rightleftharpoons O + O + M(M = N, O)$	$1.0E+22$	-1.50	59500
$O_2 + M \rightleftharpoons O + O + M(M = N_2^+, O_2^+, NO^+)$	$2.0E+21$	-1.50	59500
$O_2 + M \rightleftharpoons O + O + M(M = N^+, O^+)$	$1.0E+22$	-1.50	59500
$NO + M \rightleftharpoons N + O + M(M = N_2, O_2, NO)$	$5.0E+15$	0.00	75500
$NO + M \rightleftharpoons N + O + M(M = N, O)$	$1.1E+17$	0.00	75500
$NO + M \rightleftharpoons N + O + M(M = N_2^+, O_2^+, NO^+)$	$5.0E+15$	0.00	75500
$NO + M \rightleftharpoons N + O + M(M = N^+, O^+)$	$1.1E+17$	0.00	75500
Electron Impact Ionization			
$N + e \rightleftharpoons N^+ + e + e$	$2.5E+34$	-3.82	168600
$O + e \rightleftharpoons O^+ + e + e$	$3.9E+33$	-3.78	158500
Exchange			
$N_2 + O \rightleftharpoons NO + N$	$6.4E+17$	-1.00	38400
$NO + O \rightleftharpoons O_2 + N$	$8.4E+12$	0.00	19450
Dissociative Recombination			
$N + O \rightleftharpoons NO^+ + e$	$5.3E+12$	0.00	31900
$N + N \rightleftharpoons N_2^+ + e$	$2.0E+13$	0.00	67500
$O + O \rightleftharpoons O_2^+ + e$	$1.1E+13$	0.00	80600
Charge Exchange			
$O^+ + N_2 \rightleftharpoons N_2^+ + O$	$9.1E+11$	0.36	22800
$O^+ + NO \rightleftharpoons N^+ + NO$	$1.4E+05$	1.90	15300
$NO^+ + O_2 \rightleftharpoons O_2^+ + NO$	$2.4E+13$	0.41	32600
$NO^+ + N \rightleftharpoons N_2^+ + O$	$7.2E+13$	0.00	35500
$NO^+ + O \rightleftharpoons N^+ + O_2$	$1.0E+12$	0.50	77200
$O_2^+ + N \rightleftharpoons N^+ + O_2$	$8.7E+13$	0.14	28600
$O_2^+ + N_2 \rightleftharpoons N_2^+ + O_2$	$9.9E+12$	0.00	40700
$NO^+ + N \rightleftharpoons O^+ + N_2$	$3.4E+13$	-1.08	12800
$NO^+ + O \rightleftharpoons O_2^+ + N$	$7.2E+12$	0.29	48600

where the values of $k_{eq}\,(T_c)$ are obtained by curve fits as follows

$$K_{eq} = \exp\left[A_1\left(\frac{T_c}{10^4}\right) + A_2 + A_3 \ln\left(\frac{10^4}{T_c}\right) + A_4\left(\frac{10^4}{T_c}\right) + A_5\left(\frac{10^4}{T_c}\right)^2\right] \quad . \tag{14}$$

The coefficients A_1, A_2, A_3, A_4 and A_5 are functions of the flow particle number density within the range of the data tabulated in Park (1989). The possible reactions and the values of forward reaction ratecoefficients are available in Table 1. The coefficients M represent the third species in the dissociation reactions.

3. NUMERICAL FORMULATION

3.1 Spatial discretization

The Navier-Stokes equations are solved using the LeMANS parallel code developed at University of Michigan (Scalabrin, 2007; Martin *et al.*, 2012). The solver employs the finite volume method with a cell-centered approach. In this work, axisymmetric flows are computed using meshes solely composed of quadrilaterals in order to better resolve the boundary layers and shock waves present in hypersonic flows.

The inviscid fluxes across cell faces are discretized using a modified version of the Steger-Warming flux vector splitting scheme (MacCormack and Candler, 1989) which is less dissipative and yields better results along boundary layers. The

method switches to the original Steger and Warming (1981) scheme at shock waves by using a pressure switch. A second-order reconstruction of the inviscid fluxes is implemented as discussed in Scalabrin (2007). The viscous fluxes are calculated using a second-order centered scheme that combines properties at cell centers and the nodes. The property values at the nodes are calculated using a simple average of the cell values that share the node. Use of this method increases the stencil employed in the derivative calculations in order to avoid loss of accuracy when using unstructured meshes. No-slip velocity boundary conditions with non-catalytic isothermal walls are applied along the solid surfaces.

3.2 Treatment of source term

The spatial discretization of the source term is the same as that used to calculate the viscous flux terms. The values of properties on the left and right sides of a volume face are obtained using the values on the centroid of the respective volume and also the values of properties on the nodes that make up the control volume (Jawahar and Kamath, 2000). Forward and backward chemical reaction rates can achieve large values depending on the control volume temperature, especially for low equilibrium constant values k_{eq} (Park, 1988). Another numerical problem associated with the source term of chemical reaction is related to the densities of chemical species, which need to be positive. Negative values of densities of chemical species cause the source terms to change signs, what leads to numerical instabilities.

In order to overcome any problems in the calculation of source terms, chemical reaction rates are numerically obtained using a modified temperature discussed in Scalabrin (2007) as

$$T^{'} = \frac{1}{2}\left[(T + T_{min}) + \sqrt{(T - T_{min})^2 + \epsilon^2}\right] . \tag{15}$$

In the equation above, T_{min} and ϵ are user defined values and for the present studies, $T_{min} = 800K$ and $\epsilon = 80$ following the previous reference.

3.3 Time discretization

Numerical instabilities may appear with the use of explicit methods for time integration of the Navier-Stokes equations including source terms with chemical reactions. In such cases, the time step restriction arising from numerical stiffness does not allow an acceptable iteration time for achieving solution convergence (Hirsch, 2007). Since we sought steady state flow solutions, an alternative to avoid this kind of problem is to use implicit schemes for time integration of the equations. This approach improves efficiency and robustness, allowing larger time steps while avoiding the growth of numerical instabilities. In this work, the time integration is performed using a line implicit method (Venkatakrishnan, 1995).

4. RESULTS

This section includes an aerothermodynamic analysis of the SARA reentry satellite along the reentry path of the satellite from an altitude of 90 km to an altitude of 30 km from the Earth surface. This altitude range was chosen because it encompasses the phase of greatest intensity of heat transfer from the flow to the vehicle's surface, constituting itself as the most critical conditions for the thermal protection of the satellite.

Figure 2 shows the path of atmospheric reentry with the variation of speed as a function of altitude for the SARA vehicle from its orbit to landing on the surface of planet Earth. The discrete points in the graph identify the locations considered in the trajectory where the numerical simulations were carried out. The actual reentry procedure starts at an altitude of 125 km, with a speed of 7800 m/s, where the flow is sufficiently thin.

Figure 3 shows a mesh composed of 61,000 control volumes. The present numerical tool allows simulations of fully unstructured grids. However, to better resolve the boundary layers and shock waves appearing in the flows of interest, all mesh configurations tested are composed solely of quadrilaterals. A mesh refinement study was previously performed and converged steady-state solutions are presented along this section. Results are obtained for the mesh shown in Fig. 3 which has a maximum cell Reynolds number $Re_{cell} = Re_\infty \times \Delta n/R_n \approx 5$ for the highest Reynolds number considered in the simulations at $H = 30$ km. Here, Δn refers to the smallest normal grid distance on the wall. Therefore, we follow the best practices in terms of mesh resolution for high-speed flows as suggested by Qu *et al.* (2019). In order to validate the results obtained in this study, Fig 4 compares the present solutions with those obtained by direct simulation Monte Carlo (DSMC) Santos (2012). Results are compared in terms of heat transfer coefficient and pressure coefficient on the satellite surface for the altitude of 90 km under the same conditions. Results obtained at lower altitudes are not provided in this reference due to the inherent costs of DSMC and, to the knowledge of the authors, Navier-Stokes solutions for the other points of the SARA reentry path are not available in literature.

In Fig 4(a) it is possible to observe an excellent agreement between the results for heat transfer coefficient, $C_h = 2q_w/\rho_\infty U_\infty^3$, obtained by the present numerical simulation tool and those computed by DSMC. Although at an altitude of 90 km the flow is at the limit between the continuous and rarefied regimes, with a Knudsen number of the order $Kn \approx 0.1$,

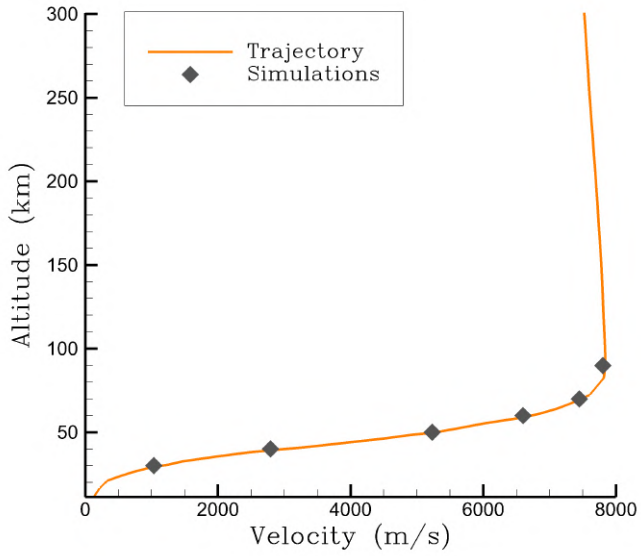

Figure 2. Reentry trajectory and simulation points of the SARA satellite.

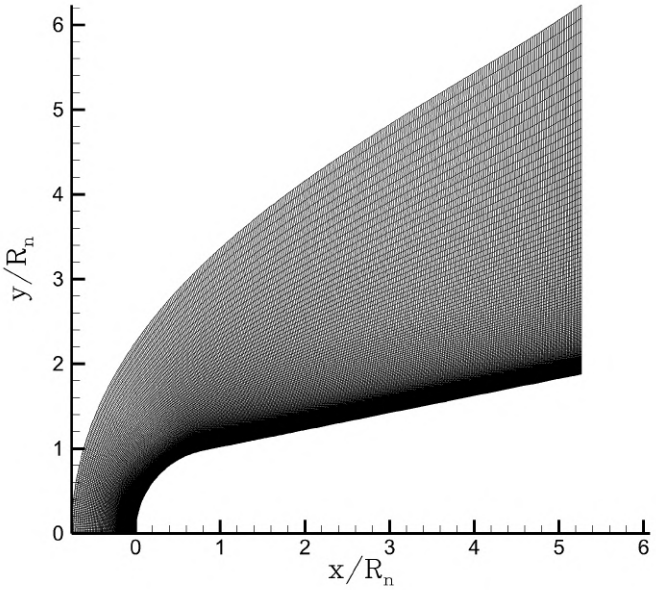

Figure 3. Computational grid topology over the Brazilian satellite SARA.

the Navier-Stokes model is still capable of providing accurate results for the heat transfer rate over the vehicle surface.

In figure 5 it is possible to observe the contours of the translational-rotational temperature mode T_{tr} for the reactive flow and the temperature T for the inert flow. It is important to note that the inert flow considers the thermodynamic balance between the temperature modes and, therefore, the temperature is described by a single value T, called thermodynamic temperature. The topology and thermal characteristics of the flow during the reentry path of the SARA satellite can be easily visualized through the temperature contours. There is a similarity in the thermal signature of reactive and inert flows at the beginning of the 90 km altitude, as can be seen in the figures 5(a) and (b). There is a small, almost imperceptible, difference in the position of the shock wave in the inert flow when compared to the reactive flow for this altitude. Such difference is visualized more easily for an altitude of 60 km in figures 5(c) and (d). Here, the difference in flow topology from the reactive to the inert flow is clear. In the reactive flow, the thickness of the shock layer is approximately 1/3 of that in the inert flow. The chemical reactions are more intense in this altitude range and drastically reduce the temperature inside the shock layer for the reactive flow. The same behavior of thermal similarity between reactive and

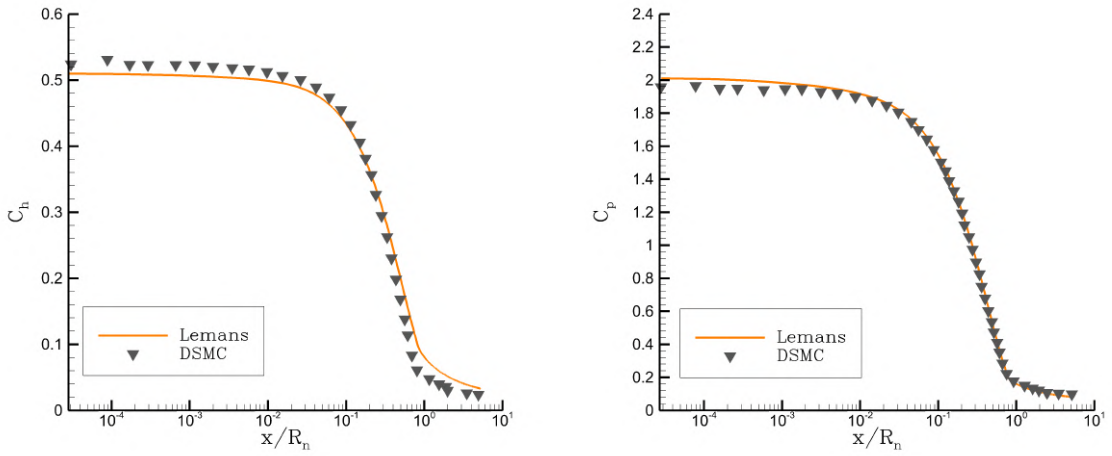

(a) Heat transfer coefficient (C_h) (b) Pressure coefficient (C_p)

Figure 4. Comparison of the present results with those obtained by DSMC Santos (2012) for 90 km altitude.

inert flows can be observed at an altitude of 30 km, as shown in figures 5(e) and (f). For this lower altitude, reactive and inert flows appear similar again.

The graphs in figure 6 show the mass fraction of the chemical species present in the air mixture along the axisymmetric stagnation line of the flow over the SARA vehicle. These results allows an assessment of the chemical behavior of the mixture when subjected to extreme temperature conditions inside the shock layer. As previously observed for the temperature contours, the flow at an altitude of 90 km behaves inertly under conditions of low density even when submitted at high temperatures. This can be confirmed in figure 6(a) that shows that the chemical dissociation reactions are practically nonexistent. In this case, the gas mixture remains as the initial composition of $76,3\%$ of nitrogen and $23,7\%$ of oxygen throughout the entire stagnation line, even when subjected by a strong shock wave.

At an altitude of 70 km, the thermal flow conditions are sufficient to induce dissociation reactions of nitrogen N_2 and oxygen O_2 molecules. Approximately 45% of the N_2 molecules are completely dissociated, while nearly 100% of the O_2 molecules are completely dissociated within the shock layer. In this dissociation process, the nitrogen and oxygen atoms remain practically free, while an insignificant portion of these atoms recombine to form the nitrogen monoxide molecule, as can be seen in figure 6(b).

As the satellite trajectory descends to altitudes less than 60 km, the amount of dissociated nitrogen also reduces, until at an altitude of 50 km. For these altitudes, the mass fraction of the nitrogen molecule reduces approximately by only 11% of the original fraction of $76,3\%$. The dissociation of the oxygen molecule remains complete in this range of altitudes. It is also possible to see in figures 6(c) and (d) the proportional reduction in the increase in the mass fraction of the free nitrogen atoms. On the other hand, there is also an increase in the production of nitrogen monoxide between the altitudes of 70 km and 50 km.

Upon penetrating the stratosphere, between altitudes of 40 and 30 km, the flow again behaves as an inert gas as shown in figures 6(e) and (f). Here, it is observed that the original mass fraction of the air mixture remains practically constant throughout the frontal region of the vehicle until reaching the surface of the capsule.

5. CONCLUSIONS AND ADDITIONS TO THE FINAL PAPER

In the present investigation, hypersonic reacting and non-reacting gas flows over the Brazilian reentry satellite SARA are performed for a trajectory ranging from 90 to 30 km altitude. These conditions simulate the atmospheric reentry of planet Earth. Numerical simulations are conducted for different flow conditions where thermodynamic non-equilibrium occurs. The Navier-Stokes equations are solved including source terms that model the chemical reactions occurring in the present high-enthalpy flows. A two-temperature model is applied to individually account for the translational and rotational modes, and the vibrational and electronic modes. The atmosphere of Earth is modeled by a gas mixture consisting of nitrogen $N2 = 76.3\%$ and oxygen $O2 = 23.7\%$.

Numerical simulations show that the chemical reactions play a important role in the reduction of temperature inside the shock layer for a certain altitude range. The reduction in the translational temperature mode is mainly caused by the gas mixture dissociation process where part of the flow energy is used to dissociate the air around the vehicle producing new species as atoms of nitrogen, oxygen and recombinations such as nitrogen monoxide. The condition of reentry at 70 and 60 km altitude is severe enough to induce relevant chemical reactions to alter the temperature distribution. This effect

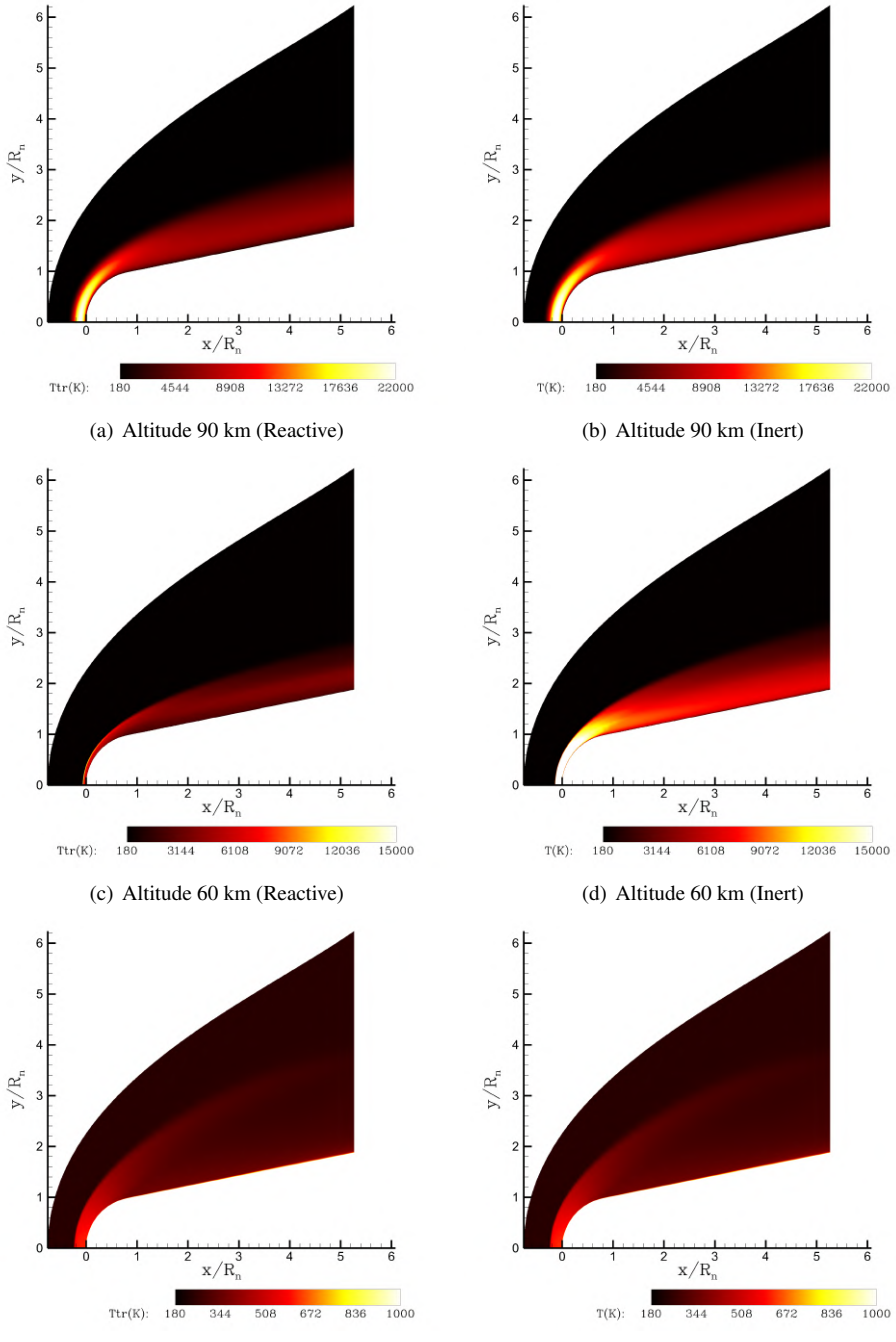

(a) Altitude 90 km (Reactive)

(b) Altitude 90 km (Inert)

(c) Altitude 60 km (Reactive)

(d) Altitude 60 km (Inert)

(e) Altitude 30 km (Reactive)

(f) Altitude 30 km (Inert)

Figure 5. Comparison of temperature contours considering reactive and inert flows for altitudes varying between 90 km and 30 km.

directly impacts on the calculation of the surface heat flux distribution. In the final version of the paper, a comparison between translational and vibrational modes will be presented as well as a comparison between the surface heat fluxes computed by inert and reactive flows.

6. ACKNOWLEDGEMENTS

The authors gratefully acknowledge the support for the present research provided by Conselho Nacional de Desenvolvimento Científico e Tecnológico, CNPq, under the Research Grants No. 309985/2013-7, 304335/2018-5 and 407842/2018-7. The work is also supported by computational resources of the Center for Mathematical Sciences Applied to Industry (CeMEAI) funded by Fundação de Amparo à Pesquisa do Estado de São Paulo, FAPESP, under the Research Grant No. 2013/07375-0. FAPESP Research Grant No. 2013/08293-7 is also acknowledged by the authors.

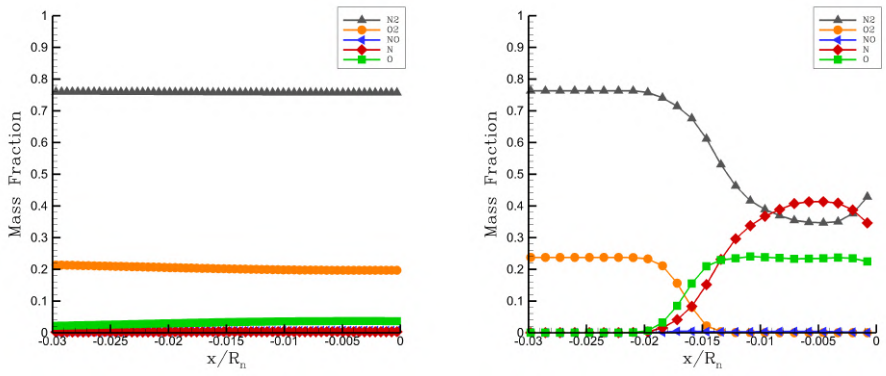

(a) Altitude 90 km

(b) Altitude 70 km

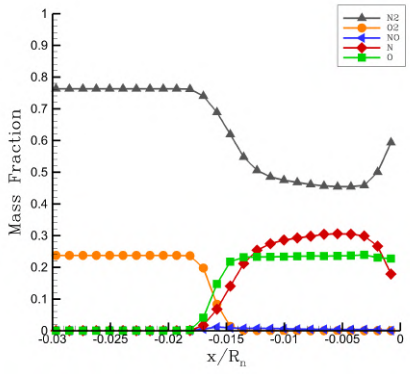

(c) Altitude 60 km

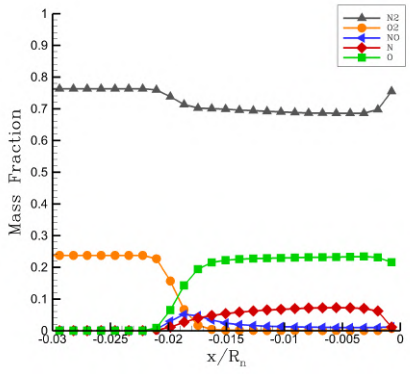

(d) Altitude 50 km

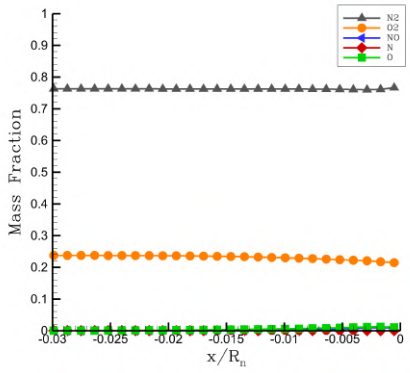

(e) Altitude 40 km

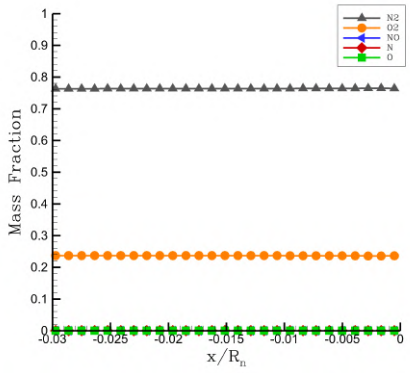

(f) Altitude 30 km

Figure 6. Mass fraction of neutral species along the stagnation line for altitudes ranging from 90km to 30km.

7. REFERENCES

Bobylev, A.V., 1982. "The chapman-enskog and grad methods for solving the boltzmann equation". In *Akademiia Nauk SSSR Doklady*. Vol. 262, pp. 71–75.

Bouyahiaoui, Z., Haoui, R., Zidane, A. and Nouiri, A., 2020. "Prediction of the flow field and convective heating during space capsule reentry using an open source solver". *International Journal of Heat and Mass Transfer*, Vol. 148, p. 119045. ISSN 0017-9310. doi:https://doi.org/10.1016/j.ijheatmasstransfer.2019.119045.

Hirsch, C., 2007. *Numerical computation of internal and external flows: The fundamentals of computational fluid dynamics*. Elsevier.

Jawahar, P. and Kamath, H., 2000. "A high-resolution procedure for euler and navier–stokes computations on unstructured grids". *Journal of Computational Physics*, Vol. 164, No. 1, pp. 165–203. doi:10.1006/jcph.2000.6596.

Kim, J.G., Kang, S.H. and Park, S.H., 2020. "Thermochemical nonequilibrium modeling of oxygen in hy-

personic air flows". *International Journal of Heat and Mass Transfer*, Vol. 148, p. 119059. doi: https://doi.org/10.1016/j.ijheatmasstransfer.2019.119059.

MacCormack, R.W. and Candler, G.V., 1989. "The solution of the navier-stokes equations using gauss-seidel line relaxation". *Computers & fluids*, Vol. 17, No. 1, pp. 135–150. doi:10.1016/0045-7930(89)90012-1.

Martin, A., Scalabrin, L.C. and Boyd, I.D., 2012. "High performance modeling of atmospheric re-entry vehicles". *Journal of Physics: Conference Series*, Vol. 341, p. 012002. doi:10.1088/1742-6596/341/1/012002.

Niu, Q., Yuan, Z., Dong, S. and Tan, H., 2018. "Assessment of nonequilibrium air-chemistry models on species formation in hypersonic shock layer". *International Journal of Heat and Mass Transfer*, Vol. 127, pp. 703 – 716. ISSN 0017-9310. doi:https://doi.org/10.1016/j.ijheatmasstransfer.2018.07.007.

Park, C., 1988. "Assessment of a two-temperature kinetic model for dissociating and weakly ionizing nitrogen". *Journal of Thermophysics and Heat Transfer*, Vol. 2, No. 1, pp. 8–16. doi:10.2514/3.55.

Park, C., 1989. "Assessment of two-temperature kinetic model for ionizing air". *Journal of Thermophysics and Heat Transfer*, Vol. 3, No. 3, pp. 233–244. doi:10.2514/3.28771.

Park, C., 1993. "Review of chemical-kinetic problems of future nasa missions. i-earth entries". *Journal of Thermophysics and Heat transfer*, Vol. 7, No. 3, pp. 385–398. doi:10.2514/3.431.

Qu, F., Chen, J., Sun, D., Bai, J. and Zuo, G., 2019. "A grid strategy for predicting the space plane's hypersonic aerodynamic heating loads". *Aerospace Science and Technology*, Vol. 86, pp. 659 – 670. ISSN 1270-9638.

Riccio, A., Raimondo, F., Sellitto, A., Carandente, V., Scigliano, R. and Tescione, D., 2017. "Optimum design of ablative thermal protection systems for atmospheric entry vehicles". *Applied Thermal Engineering*, Vol. 119, pp. 541 – 552. ISSN 1359-4311. doi:https://doi.org/10.1016/j.applthermaleng.2017.03.053.

Santos, W.F., 2012. "Aerothermodynamic analysis of a reentry brazilian satellite". *Brazilian Journal of Physics*, Vol. 42, No. 5-6, pp. 373–390.

Scalabrin, L., 2007. *Numerical simulation of weakly ionized hypersonic flow over reentry capsules*. Ph.D. thesis, University of Michigan.

Steger, J.L. and Warming, R., 1981. "Flux vector splitting of the inviscid gasdynamic equations with application to finite-difference methods". *Journal of Computational Physics*, Vol. 40, No. 2, pp. 263–293. doi:10.1016/0021-9991(81)90210-2.

Venkatakrishnan, V., 1995. "Implicit schemes and parallel computing in unstructured grid cfd". Technical report, NASA Report 195071.

Vincenti, W. and Kruger, C., 1982. *Introduction to physical gas dynamics*. Krieger.

Wang, X., Yan, C., Zheng, Y. and Li, E., 2017. "Assessment of chemical kinetic models on hypersonic flow heat transfer". *International Journal of Heat and Mass Transfer*, Vol. 111, pp. 356 – 366. ISSN 0017-9310. doi: https://doi.org/10.1016/j.ijheatmasstransfer.2017.03.102.

Wilke, C., 1950. "A viscosity equation for gas mixtures". *The journal of chemical physics*, Vol. 18, No. 4, pp. 517–519. doi:10.1063/1.1747673.

Yang, X., Gui, Y., Xiao, G., Du, Y., Liu, L. and Wei, D., 2020. "Reacting gas-surface interaction and heat transfer characteristics for high-enthalpy and hypersonic dissociated carbon dioxide flow". *International Journal of Heat and Mass Transfer*, Vol. 146, p. 118869. ISSN 0017-9310. doi:https://doi.org/10.1016/j.ijheatmasstransfer.2019.118869.

8. RESPONSIBILITY NOTICE

The authors are solely responsible for the printed material included in this paper.